

Amorphous IGMO/IGZO heterojunction thin-film transistors with enhanced ultraviolet detection performance

Jichun Yao(姚继春), Yiyu Zhang(张怡宇), and Xingzhao Liu(刘兴钊)

Citation : Chin. Phys. B, 2025, 34 (**5**): 057104. DOI: 10.1088/1674-1056/adb8b6
http://cpb.iphy.ac.cn; http://iopscience.iop.org/cpb

What follows is a list of articles you may be interested in

Improved RF power performance of InAlN/GaN HEMT by optimizing rapid thermal annealing process for high-performance low-voltage terminal applications

Yuwei Zhou(周雨威), Minhan Mi(宓珉瀚), Pengfei Wang(王鹏飞), Can Gong(龚灿), Yilin Chen(陈怡霖), Zhihong Chen(陈治宏), Jielong Liu(刘捷龙), Mei Yang(杨眉), Meng Zhang(张濛), Qing Zhu(朱青), Xiaohua Ma(马晓华), and Yue Hao(郝跃)
Chin. Phys. B, 2023, 32 (**12**): 127102. DOI: 10.1088/1674-1056/acd8a1

Modulation of Schottky barrier in XSi$_2$N$_4$/graphene (X=Mo and W) heterojunctions by biaxial strain

Qian Liang(梁前), Xiang-Yan Luo(罗祥燕), Yi-Xin Wang(王熠欣), Yong-Chao Liang(梁永超), and Quan Xie(谢泉)
Chin. Phys. B, 2022, 31 (**8**): 087101. DOI: 10.1088/1674-1056/ac5c3b

Dynamic recombination of triplet excitons in polymer heterojunctions

Ya-Dong Wang(王亚东), Jian-Jun Liu(刘建军), Xi-Ru Wang(王溪如), Yan-Xia Liu(刘艳霞), and Yan Meng(孟艳)
Chin. Phys. B, 2020, 29 (**11**): 117101. DOI: 10.1088/1674-1056/ab9c13

Photodetectors based on two-dimensional materials and organic thin-film heterojunctions

Jiayue Han(韩嘉悦), Jun Wang(王军)
Chin. Phys. B, 2019, 28 (**1**): 017103. DOI: 10.1088/1674-1056/28/1/017103

Electrical property effect of oxygen vacancies in the heterojunction of $LaGaO_3$/$SrTiO_3$

Fu-Ning Wang(王芙凝), Ji-Chao Li(李吉超), Xin-Miao Zhang(张鑫淼), Han-Zhang Liu(刘汉璋), Jian Liu(刘剑), Chun-Lei Wang(王春雷), Ming-Lei Zhao(赵明磊), Wen-Bin Su(苏文斌), Liang-Mo Mei(梅良模)
Chin. Phys. B, 2017, 26 (**3**): 037101. DOI: 10.1088/1674-1056/26/3/037101

Amorphous IGMO/IGZO heterojunction thin-film transistors with enhanced ultraviolet detection performance

Jichun Yao(姚继春), Yiyu Zhang(张怡宇), and Xingzhao Liu(刘兴钊)†

State Key Laboratory of Electronic Thin Films and Integrated Devices, School of Integrated Circuit Science and Engineering, University of Electronic Science and Technology of China, Chengdu 611731, *China*

(Received 16 December 2024; revised manuscript received 19 February 2025; accepted manuscript online 21 February 2025)

Amorphous InGaZnO (IGZO) is a potential candidate for integrated circuits based on thin-film transistors (TFTs) owing to its low-temperature processability and high mobility. Amorphous InGaMgO/InGaZnO (IGMO/IGZO) heterojunction was deposited and TFTs based on IGMO/IGZO heterojunction were fabricated in this report. The energy band at the IGMO/IGZO heterojunction was characterized, and the potential well at the interface of IGZO is critical to the enhanced ultraviolet detection of the IGMO/IGZO heterojunction. Furthermore, the TFTs based on IGMO/IGZO heterojunction exhibited a high responsivity of 3.8×10^3 A/W and a large detectivity of 5.2×10^{14} Jones under 350-nm ultraviolet illumination, which will also benefit for fabrication of monolithic ultraviolet sensing chip.

Keywords: InGaZnO (IGZO), heterojunction, transistors, ultraviolet detection

PACS: 71.20.Nr, 73.20.At, 73.40.–c, 78.40.–q

DOI: 10.1088/1674-1056/adb8b6 **CSTR:** 32038.14.CPB.adb8b6

1. Introduction

Metal oxides are not only the most abundant materials in the Earth's crust, but also possess many properties in their magnetic and electronic behavior that originate from a variety of crystal structure and constituent elements.[1] So, they are important in a wide range of applications including sensors,[2] memories,[3] flat panel displays,[4] power harvesting,[5] and environmental waste management.[6] Among them, metal–oxide semiconductors are strikingly different from conventional inorganic semiconductors such as silicon and III–V compounds with respect to materials design concepts, electronic structure, charge transport mechanisms, defect states, thin-film processing, and optoelectronic properties, thereby enabling both conventional and completely new functions. As a kind of transparent materials, metal–oxide semiconductors with wide bandgap have brought to attention as active semiconductor components and can be tuned for applications where high transparency and electrical conductivity.[7,8] Thin-film transistor was fabricated by using single-crystalline thin-film transparent oxide semiconductor, $InGaO_3(ZnO)_5$, as an electron channel and amorphous hafnium oxide as a gate insulator in 2003.[9] The device exhibits an on/off current ratio of $\sim 10^6$ and a field-effect mobility of ~ 80 $cm^2\cdot V^{-1}\cdot s^{-1}$ at room temperature. Although this result provides a step toward the realization of transparent electronics. Synthesis and fabrication of these materials, as well as processing into particular device structures to suit a specific application, such as flexible electronics is still a challenge, owing to a trade-off between processing temperature and device performance. Amorphous oxide semiconductor from the In–Ga–Zn–O system (IGZO) was proposed in 2004.[10] The main advantages of amorphous IGZO-based TFTs include high resolution, lower leakage current, less power consumption, and less noise influence for display.[11] So, it has been in mass-production since 2012 for active-matrix liquid crystal display due to the huge investment of several high-profile companies. And as a better semiconductor platform than a-Si:H, IGZO is currently migrating towards other applications like: photodetectors,[12] memories,[13] x-ray sensors,[14] and biosensors.[15] Although huge success has been achieved in IGZO platform, another challenge is to improve the electron mobility of the complex amorphous oxide materials.[16–18] Currently the mobility of about 10 $cm^2\cdot V^{-1}\cdot s^{-1}$ at room temperature is still low a bit.

The two-dimensional electron gas (2DEG) in heterojunctions has been proven to a successful system to improve the mobility of semiconductors. The AlGaAs/GaAs and AlGaN/GaN heterojunctions have already gone commercial for active microwave devices to well meet mobile communication.[19] The 2DEG system with a carrier density of 2×10^{14} cm^{-2} at the $LaAlO_3/SrTiO_3$ interface was discovered in 2004 by Ohtomo and Hwang,[20] and this 2DEG system can be completely deplete with gate voltage smaller than a few voltages.[21] Although the results demonstrate substantial progress in the creation of new functionality by controlling materials down to the atomic level, the relatively low electron mobility of about 10 $cm^2\cdot V^{-1}\cdot s^{-1}$ at room temperature limited its electronic devices fabrication. As an important oxide semiconductor, ZnO/ZnMgO heterostructures were grown,

†Corresponding author. E-mail: xzliu@uestc.edu.cn

© 2025 Chinese Physical Society and IOP Publishing Ltd. All rights, including for text and data mining, AI training, and similar technologies, are reserved.

in which the MgZnO layer acts as a potential barrier for the 2DEG in the adjacent ZnO layer. The electron density was controlled in a range of 0.7×10^{12} cm^{-2} to 3.7×10^{12} cm^{-2}, and the electron mobility was in a range of 150 cm$^2\cdot$V$^{-1}\cdot$s^{-1} to 160 cm$^2\cdot$V$^{-1}\cdot$s^{-1} at room temperature by tuning the magnesium content in the barriers and the growth polarity.[22] However, single-crystal ZnO and ZnMgO thin films with eliminated defects is necessary to demonstrate such high electron mobility. So, the high processing temperature limits the fabrication of flexible electronic devices based on ZnO/ZnMgO heterojunction.

Because of the compositional complexity, layered crystal structure $RAMO_4$ compounds with R^{3+} = In or Sc, A^{3+} = Al or Ga, and M^{2+} = Cd, Mg, or Zn, lead to a wide range of bandgap value.[23] As a member of $RAMO_4$, wide bandgap semiconductor $InGaZnO_4$ (IGZO) is a good candidate for heterojunction with plenty of potential barrier choice. Here, thin-film transistor (TFT) based on heterojunction of amorphous $InGaMgO_4$ (IGMO) as a potential barrier layer and IGZO as a channel layer is reported. An improved ultraviolet detection performance was achieved in the TFT based on IGMO/IGZO heterojunction. The energy band alignment was studied to show possible 2DEG system at the IGMO/IGZO interface. The experiment results showed that amorphous IGMO/IGZO heterojunction is critical to flexible electronics.

2. Experimental details

Bottom-gated IGMO/IGZO TFT was fabricated on SiO_2 (300 nm)/Si substrates, which was ultrasonically cleaned in acetone, alcohol, and deionized water successively and then blown dry by pure nitrogen gas before deposition. Amorphous IGZO and IGMO films were deposited on the substrates at room temperature by radio-frequency (RF) magnetron sputtering using IGZO and IGMO ceramic targets with the working pressure of 3.8 mTorr (1 Torr = 1.33322×10^2 Pa) and RF power of 80 W. The 100-nm thick IGZO layer and 100-nm thick IGMO were sputtered in order in a mixed Ar/O_2 atmosphere with the ratio of the Ar and O_2 gas flow of 10 sccm:1.1 sccm. In addition, patterned channel layer was defined by photolithography technique and etched by dilute hydrochloric acid solution (dilute in a 1:10 ratio of hydrochloric acid to water). The Ti/Au electrodes deposition was carried out in an electron-beam evaporation process after photolithography. Then, lift-off process removed photoresist. Finally, the samples were sent to the rapid annealing equipment for achieving a good Ohmic contact performance between the channel and the electrodes with annealing temperature of 350 °C and annealing time of 300 s. Additionally, the effective illumination area of the devices is 5×10^{-4} cm^2.

Tauc plot was derived from the transmission spectra measured by ultraviolet-visible spectrophotometer (PERSEE TU-1810). XPS measurements were performed on an XSAM800 x-ray photoelectron spectrometer using Al $K\alpha$ (1486.6 eV) as a monochromatic x-ray source. The binding energy was calibrated by C 1s at 284.8 eV. The electronic and photoelectronic measurements were performed in a probe station (1100B-M, Cascade) equipped with a semiconductor characterization system (4155B, Agilent) at room temperature.

3. Result and discussion

Figure 1(a) shows the fabrication process of the IGMO/IGZO TFT. Figure 1(b) shows the cross-section SEM image of IGMO/IGZO heterojunction deposited on SiO_2/Si substrate. We can observe obvious layers, from top to bottom, IGMO, IGZO, and SiO_2 in order. Figure 2(a) shows the Tauc plot of IGZO and IGMO films. The ultraviolet-visible transmission spectra of the IGZO and IGMO were measured and the energy bandgaps of the samples were determined by the Tauc method, that is, extrapolating the linear region of the incident photon energy ($h\nu$) *versus* $(\alpha h\nu)^{1/2}$ to the horizontal axis. The corresponding absorption coefficient (α) was obtained from the following equation:[24]

$$\alpha = \frac{1}{t}\ln(1/T), \tag{1}$$

where t and T are the thicknesses of the sample and transmission, respectively. Consequently, the energy bandgaps (E_G) of IGZO and IGMO are determined to be 3.0 eV and 3.9 eV, respectively. Larger bandgap in IGMO film is attributed to the strength of the Mg–O bonds compared to Zn–O bonds. We speculated that intense photo-absorption of the IGMO layer would dominantly be in the ultraviolet region due to its large E_G, while the contribution of the existing IGZO layer to the ultraviolet absorption is not expected to be significant due to the narrow E_G, relatively. The x-ray diffraction (XRD) patterns demonstrate that there

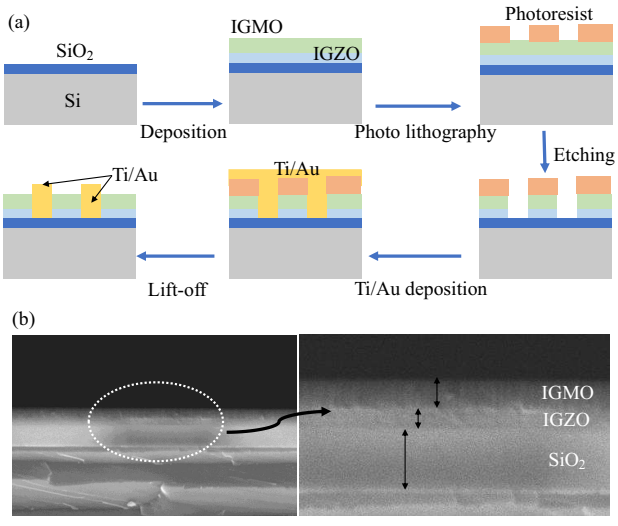


Fig. 1. (a) The fabrication process of the IGMO/IGZO TFT. (b) The cross-section scanning electron microscope (SEM) image of IGMO/IGZO heterojunction deposited on SiO_2/Si substrate.

are no obvious diffraction peaks except for the two strong Si peaks related to the substrates, which indicates annealing IGZO and IGMO films are amorphous states, as shown in Fig. 1(b). In addition, IGMO/IGZO heterojunction also exhibits typical amorphous state, as shown in Fig. S1 in supporting materials.

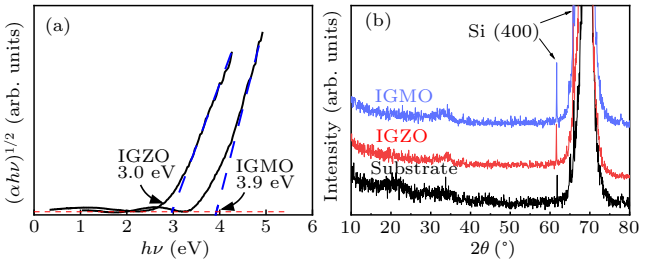


Fig. 2. (a) Tauc plot, $(\alpha h\nu)^{1/2}$ as a function of photon energy $h\nu$, where ν is the photon frequency, indicating the energy bandgap of IGZO (3.0 eV) and IGMO (3.9 eV). (b) The XRD pattern.

To better understand the IGMO/IGZO heterojunction interface, x-ray photoelectron spectroscopy (XPS) studies were carried out for IGZO bulk, IGMO bulk, and IGMO/IGZO heterojunction. The XPS analysis revealed the constituent elements in IGMO and IGZO bulk. The Zn $2p_{3/2}$ peak was observed at 1021.63 eV in IGZO bulk, and E_V is 2.49 eV calculated by linear epitaxy method, as shown in Fig. 3(a). Similarly, Mg 2p peak was identified at 50.22 eV for IGMO bulk and with an E_V of 3.61 eV, as shown in Fig. 3(b). The Zn $2p_{3/2}$ peak and Mg 2p peak at the IGMO/IGZO heterojunction interface are shown in Fig. 3(c). The Zn $2p_{3/2}$ peak is located at 1021.87 eV, with a 0.24-eV higher binding energy for IGZO bulk, indicating that the energy band bends downwards from the IGZO bulk to the interface. In contrast, the Mg 2p peak centered at 49.49 eV, where a clear shift of 0.73 eV to a lower binding energy was also observed for IGMO bulk, resulting in the upward bending of energy band at the interface. Therefore, the binding energy distinction between Zn $2p_{3/2}$ peak and Mg 2p peak at heterojunction interface was calculated to be 972.38 eV. Equation (2) is used to calculate ΔE_V,[25] which is 0.15 eV.

$$\Delta E_V = \left(E_{CL}^{IGZO} - E_{VBM}^{IGZO}\right) - \left(E_{CL}^{IGMO} - E_{VBM}^{IGMO}\right) - \Delta E_{CL}, \quad (2)$$

where E_{CL}^{IGZO} and E_{VBM}^{IGZO} represent the characteristic peak and the valence-band maximum in the IGZO bulk, respectively, while E_{CL}^{IGMO} and E_{VBM}^{IGMO} represent the characteristic peak and valence-band maximum of IGMO bulk, respectively. ΔE_{CL} represents the distinction of binding energy of the characteristic peak at the IGMO/IGZO heterojunction interface, which can be defined as $\Delta E_{CL} = E_{CL}^{IGZO} - E_{CL}^{IGMO}$. Furthermore, Ga $2p_{3/2}$ peak and In $3d_{5/2}$ peak are also used as characteristic peaks to calculate the ΔE_V at the heterojunction interface in the same way. The calculated average value of ΔE_V at the IGMO/IGZO heterojunction interface is 0.09 eV. The ΔE_C at the IGMO/IGZO heterojunction interface can be calculated by the following equation:

$$\Delta E_C = E_G^{IGMO} - E_G^{IGZO} - \Delta E_V, \quad (3)$$

where E_G^{IGMO} and E_G^{IGZO} are energy bandgaps of IGMO and IGZO, respectively. Finally, the value of ΔE_C was determined to be 0.83 eV. Based on those data, band diagram of IGZO and IGMO before heterojunction formation is shown in Fig. S2.

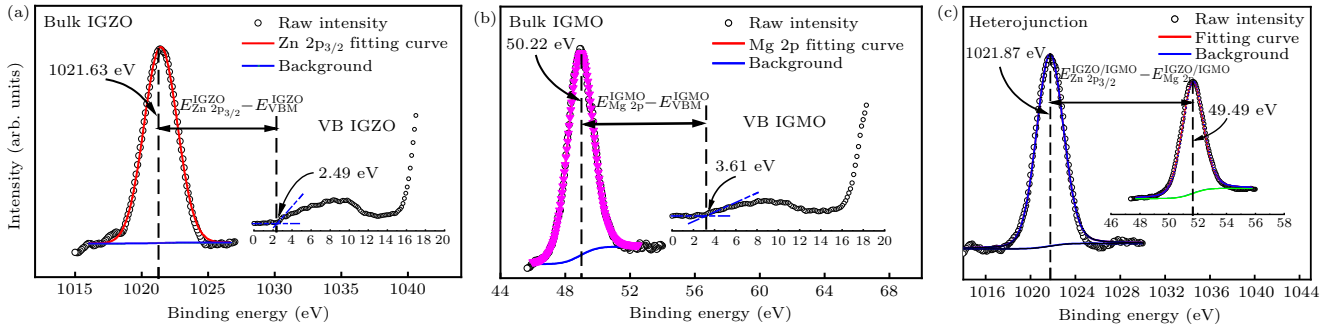


Fig. 3. XPS results: (a) valence band of InGaZnO bulk and Zn $2p_{3/2}$ peak at 1021.63 eV, (b) valence band for InGaMgO bulk and Mg 2p peak at 50.22 eV, (c) Zn $2p_{3/2}$ peak at 1021.87 eV and Mg 2p peak at 49.49 eV in the IGMO/IGZO heterojunction.

The schematic energy band alignment with band bending at the IGMO/IGZO heterojunction interface is shown in Fig. 4(a). The IGMO/IGZO heterojunction is the type I (straddling gap) heterojunction.[26] The energy band bends downwards from the IGZO bulk to the heterojunction interface, forming a potential well of 0.24 eV. While the energy band bends upwards from the IGMO bulk to the heterojunction interface, forming a potential barrier of 0.83 eV. Considering that both IGZO and IGMO are n-type semiconductors, the electrons in the conduction band are easily accumulated at the IGMO/IGZO heterojunction interface. In order to keep thermal equilibrium, electrons will transfer from IGMO to IGZO at the interface. Then electrons were confined to the potential well after reaching the IGZO layer. This energy band structure at the interface is beneficial to bound electrons. In addition, the schematic energy band alignment, which does not take in the factor of band bending, is shown in Fig. 4(b). Here, the ΔE_V is directly determined by the difference E_V between the

two materials. It can be found that the energy band structure at the IGMO/IGZO interface changes from the type-I heterojunction to the type-II (staggered gap) heterojunction, While the ΔE_V increases to 1.12 eV, and the ΔE_C decreases to −0.2 eV. Obviously, this negative ΔE_C may make it impossible for heterojunction to bound electrons. When the type-I heterojunction forms, electrons cross the potential barrier on the side of IGMO and enter into the potential well on the side of IGZO. Due to the existence of the potential barrier, electrons in IGZO layer can only move in the potential well at the heterojunction interface, not vertically between layers. Therefore, it is the fact that the mobility of the device increases greatly when the energy band structure is formed at the IGMO/IGZO heterojunction interface. In addition, based on such an energy band alignment, it is suggested that the electrons are confined in the potential well to probably generate 2DEG.[27,28]

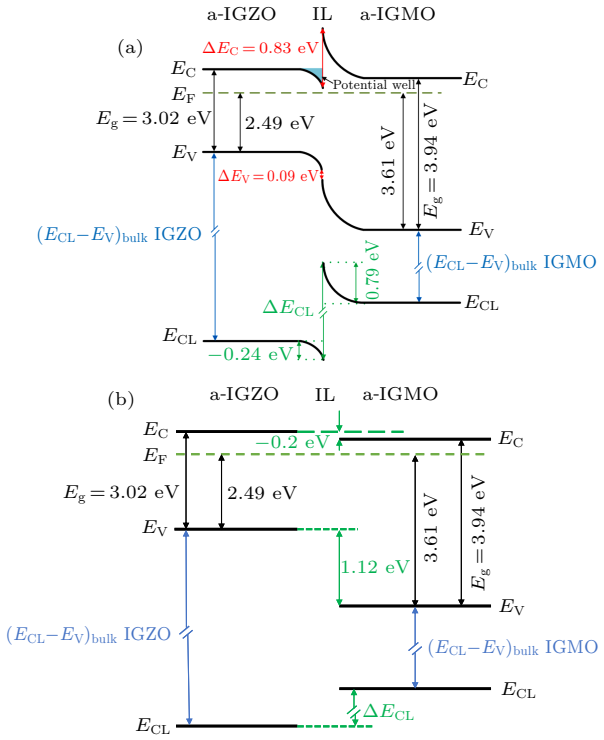


Fig. 4. The schematic energy band alignment of the IGMO/IGZO heterojunction based on the Tauc plots and XPS analysis: (a) with band bending and (b) without band bending.

Figures 5(a) and 5(b) show representative photoelectronic characteristics of TFTs with and without IGMO layer under illumination with a fixed light power density of 66.7 μW·cm^{-2} at different wavelengths (250 nm, 300 nm, 350 nm, 400 nm, 450 nm, 500 nm, 550 nm, and 600 nm). At V_{DS} = 5 V and V_{GS} = 0 V, IGMO/IGZO TFT shows a high photocurrent (I_{photo}) of ∼ 10^{-4} A, leading to a large photo-to-dark current ratio (I_{photo}/I_{dark}) as high as 1.6×10^4, which is much improved compared with that of the IGZO TFT (I_{photo} of ∼ 10^{-6} A and I_{photo}/I_{dark} of ∼ 6.2×10^3) under illumination at 350 nm. It is noted that there is an evident increase of the dark current in IGMO/IGZO TFT in comparison to IGZO TFT, which is attributed to potential well at the heterojunction interface binding the channel electrons. The band alignment reveals that electrons are easily confined in the potential well at the interface, which makes it more difficult to deplete the electrons in the channel than the single thin films, resulting in a larger dark current. In addition, IGZO shows a higher field effect mobility than IGMO in the dark, as shown in Fig. S4, which also implies that IGZO exhibits stronger electron mobility ability in conductive channel compared with IGMO. To evaluate the light sensitivity of IGZO and IGMO/IGZO TFTs, two key parameters, namely, responsivity (R) and detectivity (D^*) were extracted, which R and D^* can be described using the following equations:[29]

$$R = \frac{I_{photo} - I_{dark}}{P \times S}, \tag{4}$$

$$D^* = \frac{RS^{1/2}}{(2qI_{dark})^{1/2}}, \tag{5}$$

where I_{photo} is the current when illuminated, I_{dark} is the current without illumination, P is the light power density, S is the effective illumination area of the channel, and q is the electron charge. Figures 5(c) and 5(d) present the calculated responsivity and detectivity of TFTs as a function of wavelength at V_{DS} = 5 V and V_{GS} = 0 V. It can be seen that the photoresponse peak of the IGZO TFT is located at 400 nm, where R and D^* of the device are 38 A/W and 3.5×10^{13} Jones, respectively. The IGMO/IGZO TFT obtains dramatic improvements in D^*, specifically in R, reaching 5.2×10^{14} Jones and 3.8×10^3 A/W under illumination at 350 nm, respectively. The selective response to the wavelength is determined by the energy bandgap of the films, and the results also correspond to the Tauc plot.

Before light illumination, the TFTs work in the depletion region with a low off current since neither conductive channel nor photogenerated carriers form in this case. When photons with high energy equivalent to the bandgap illuminate the TFTs, electrons are excited from the valence band into the conduction band causing the creation of free electron–hole pairs and the neutral oxygen vacancy (V_O) are ionized, generating shallow donors (V_O^{2+}) and releasing electrons,[30–32] both of which make significant contributions to the I_{DS}. At negative gate bias, negative charges on the gate are compensated by ionized oxygen vacancies V_O^{2+} with positive charges, causing some electrons to be confined to this region, forming an undepleted channel. Therefore, I_{DS} under light illumination increases distinctly compared with that in the dark. The higher performance of IGMO/IGZO TFT makes it essential to illustrate the roles of IGZO and IGMO layers in photo response processes. The differences in photoresponse behaviors between IGMO/IGZO TFT and IGZO TFT confirmed that the IGMO acts as an ultraviolet absorption layer due to its larger

bandgap (3.9 eV). IGMO layer enables to enhance the absorption of ultraviolet to generate electrons, which derived from the generation of electron–hole pairs and ionization of V_O. IGZO is responsible for the electrons transfer in the heterojunction due to its excellent electron mobility. Moreover, an electron bound structure forms at the heterojunction interface, as mentioned above. When the IGMO/IGZO TFT is illuminated by light with sufficient energy, a large number of electrons generated in the IGMO layer will cross the potential barrier and be injected into the IGZO layer due to the band bending at the heterojunction interface, with the result that electrons can be confined at the interface, only moving in the potential well.[33] The electrons in the channel layer are extracted to the Ti/Au electrodes rapidly because of the high mobility and make a great contribution to the photocurrent gain, which is conducive to achieving a high responsivity and a high detectivity. Overall, the high mobility of IGZO film, the excellent light absorption of IGMO film and the specific electron transfer mechanism in the heterojunction are of great significance to improve the photoelectronic performance of the device. To comprehensively assess the performance of our IGMO/IGZO TFT in ultraviolet response, the comparison of photoelectronic characteristics between IGMO/IGZO TFT and IGZO-based TFTs described from previous reports is shown in Table 1. Undoubtedly, this amorphous IGMO/IGZO heterojunction TFT demonstrates enormous potential in ultraviolet detection and flexible electronic device due to its high performance and low processing temperature.

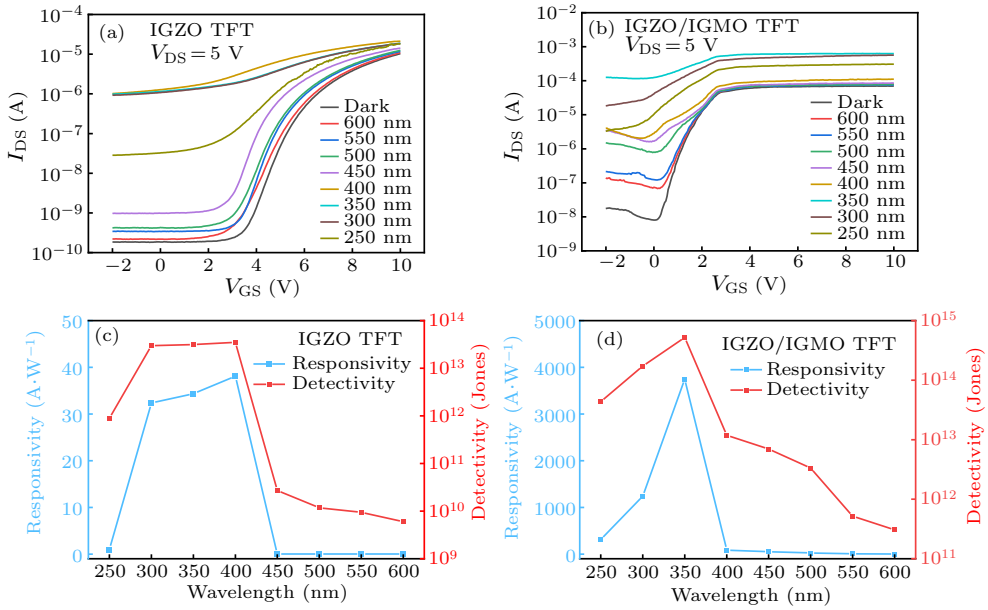


Fig. 5. TFTs illuminate by light with a power of ~ 66.7 μW·cm^{-2} at V_{DS} = 5 V. (a) Transfer characteristics of IGZO TFT. (b) Transfer characteristics of IGMO/IGZO TFT. The calculated responsivity and detectivity in various wavelengths at V_{GS} = 0 V: (c) IGZO TFT, (d) IGMO/IGZO TFT.

Table 1. The photoelectronic performance of reported TFT based on IGZO.

IGZO TFT	Wavelength (nm)	V_{GS} (V)	V_{DS} (V)	Responsivity (A/W)	Detectivity (Jones)	Ref.
IGZO with $CsPbBr_3$ quantum dots	350	–3	30	9.72	2.96×10^{12}	[33]
$CH_3NH_3PbI_3$/IGZO heterojunction	532	–1	10.1	61	9.42×10^{10}	[8]
Ga_2O_3/IGZO heterojunction	254	–5	10	8.35×10^{3}	2.59×10^{17}	[34]
IGZO TFT with DM gate	365	0	–1	126.1	6.8×10^{13}	[35]
IGZO decorated with Ag NPs and DM gate	365	0	1	1.2×10^{3}	6.7×10^{14}	[35]
IGZO only	350	0	5	32.4	3×10^{13}	this work
IGMO/IGZO heterojunction	350	0	5	3.8×10^{3}	5.2×10^{14}	this work

4. Conclusion

In summary, the IGMO/IGZO TFT shows the enhanced photoelectronic characteristics, including a high responsivity of 3.8×10^{3} A/W, and a high detectivity of 5.2×10^{14} Jones under ultraviolet illumination (350 nm, 66.7 μW·cm^{-2}) at V_{GS} = 0 V and V_{DS} = 5 V, relative to IGZO TFT. Energy band alignment of the IGMO/IGZO heterojunction reveals the existence of potential well at the interface. Electrons are confined in potential well and only move at the interface, leading to an outstanding photoelectronic performance of IGMO/IGZO TFT. It is no doubt that amorphous IGMO/IGZO heterojunction TFT is quite promising for a new generation of ultraviolet

detection.

Acknowledgement

Project supported by the Regional Innovation and Development Joint Fund of the National Nature Science Foundation of China (Grant No. U21A2071).

References

[1] Wang X, Chai Y S, Zhou L, Cao H B, Cruz C, Yang J Y, Dai J H, Yin Y Y, Yuan Z, Zhang S J, Yu R Z, Azuma M, Shimakawa Y, Zhang H M, Dong S, Sun Y, Jin C Q and Long Y W 2015 *Phys. Rev. Lett.* **115** 087601
[2] Zhu L Y, Ou L X, Mao L W, Wu X Y, Liu Y P and Lu H L 2023 *Nano-Micro Lett.* **15** 89
[3] Wang W H, Li K, Lan J, Shen M, Wang Z R, Feng X W, Yu H Y, Chen K, Li J M, Zhou F C, Lin L Y, Zhang P P and Li Y D 2023 *Nat. Commun.* **14** 6079
[4] Wang Z W, Nayak P K, Carraveo J A and Alshareef H N 2016 *Adv. Mater.* **28** 3831
[5] Sunarso J, Hashim S S, Zhu N and Zhou W 2017 *Prog. Energ. Combust.* **61** 57
[6] Ahuja T, Brighu U and Saxena K 2023 *J. Water Process Eng.* **53** 103759
[7] Chen W T and Zan H W 2012 *IEEE Electron Dev. Lett.* **33** 77
[8] Tak Y J, Kim D J, Kim W, Lee J H, Kim S J, Kim J H and Kim H J 2018 *ACS Appl. Mater. Interfaces* **10** 12854
[9] Nomura K, Ohta H, Ueda K, Kamiya T, Hirano M and Hosono H 2003 *Science* **300** 1269
[10] Nomura K, Ohta H, Takagi A, Kamiya T, Hirano M and Hosono H 2004 *Nature* **432** 488
[11] Li Y, Zhu L, Chen C S, Zhu Y, Wan C J and Wan Q 2022 *Chin. Phys. Lett.* **39** 228501
[12] Yoo H, Kim W, Kang B H, Kim H T, Park J W, Choi D H, Kim T S, Lim J H and Kim H J 2020 *ACS Appl. Mater. Interfaces* **12** 10673
[13] Hu Q L, Gu C R, Li Q J, Zhu S W, Liu S Y, Li Y, Zhang L N, Huang R and Wu Y Q 2023 *Adv. Mater.* **35** 2210554
[14] Breemen A J, Simon M, Tousignant O, Shanmugam S, Steen J, Akkerman H B, Kronemeijer A, Ruetten W, Raaijmakers R, Alving L, Jacobs J, Malinowski P E, Roose F D and Gelink G H 2020 *Npj Flexible Electron* **4** 22
[15] Yang T H, Chen T Y, Wu N T, Chen Y T and Huang J J 2017 *IEEE Trans. Electron Dev.* **64** 1294
[16] Yu Y N, Lv N N, Zhang D G, Wei Y R and Wang M X 2021 *IEEE Electron Dev. Lett.* **42** 1480
[17] Song S, Liang H L, Huo W X, Zhang G, Zhang Y H, Wang J W and Mei Z X 2024 *Chin. Phys. Lett.* **41** 068501
[18] Zhang M N, Shao Y, Wang X L, Wu X H, Liu W J and Ding S J 2020 *Chin. Phys. B* **29** 078503
[19] Hao Y, Ma X H, Mi M H and Yang L A 2021 *IEEE Microw. Mag.* **22** 34
[20] Ohtomo A and Hwang H Y 2004 *Nature* **427** 423
[21] Li L, Richter C, Paetel S, Kopp T, Mannhart J and Ashoori R C 2011 *Science* **332** 825
[22] Tsukazaki A, Ohtomo A, Kita T, Ohno Y, Ohno H and Kawasaki M 2007 *Science* **315** 1388
[23] Murat A and Medvedeva J E 2012 *Phys. Rev. B* **85** 155101
[24] Qian L X, Wu Z H, Zhang Y Y, Lai P T, Liu X Z and Li Y R 2017 *ACS Photon.* **4** 2203
[25] Kan S, Takemote S, Kaneko K, Takahashi I, Sugimoto M, Shinohe T and Fujita S 2018 *Appl. Phys. Lett.* **113** 212104
[26] Owen M H S, Bhuiyan M A, Zhou Q, Zhang Z, Pan J S and Yeo Y 2014 *Appl. Phys. Lett.* **104** 091605
[27] Lee M, Jo J, Kim Y J, Choi S, Kwon S M, Jeon S P, Facchetti A, Kim Y H and Park S K 2018 *Adv. Mater.* **30** 1804120
[28] Ji X Q, Yuan Y Z, Yin X M, Yan S Q, Xin Q and Song A M 2022 *IEEE Trans. Electron. Dev.* **69** 6783
[29] Choi H, Seo S, Lee J H, Hong S H, Song J, Kim S, Yim S Y, Lee K, Park S J and Lee S 2018 *J. Mater. Chem. C* **6** 6014
[30] Hwang J D, Yang C C and Chu C M 2017 *ACS Appl. Mater. Interfaces* **9** 23904
[31] Lee J, Kim H, Pi J, Kang S, Kwon K and Cho S H 2020 *Appl. Phys. Lett.* **117** 111103
[32] Ahn J, Ma J, Lee D, Lin Q, Park Y, Lee O, Sim S, Lee K, Yoo G and Heo J 2021 *ACS Photon.* **8** 557
[33] Yu H, Liu X Y, Yan L Z, Zou T Y, Yang H, Liu C, Zhang S D and Zhou H 2019 *Semicond. Sci. Tech.* **34** 125013
[34] Ji X Q, Yin X M, Ding Z J, Yan S Q, Zhou X Y, Zhang J W, Xin Q and Song A M 2023 *IEEE Electron. Dev. Lett.* **44** 1512
[35] Ferhati H and Djeffal F 2021 *Sensor. Actuator A Phys.* **318** 112523